



RESEARCH ARTICLE

# Simple, stable and efficient nonlinear pulse compression through cascaded filamentation in air

Tao Pu<sup>1</sup>, Kan Tian, Bo Hu, Zhongjun Wan, Linzhen He, Xuemei Yang, Han Wu<sup>1</sup>, Yang Li, Weizhe Wang, and Houkun Liang<sup>1</sup>

College of Electronics and Information Engineering, Sichuan University, Chengdu, China

(Received 17 May 2023; revised 18 July 2023; accepted 9 August 2023)

## Abstract

Nonlinear compression has become an obligatory technique along with the development of ultrafast lasers in generating ultrashort pulses with narrow pulse widths and high peak power. In particular, techniques of nonlinear compression have experienced a rapid progress as ytterbium (Yb)-doped lasers with pulse widths in the range from hundreds of femtoseconds to a few picoseconds have become mainstream laser tools for both scientific and industrial applications. Here, we report a simple and stable nonlinear pulse compression technique with high efficiency through cascaded filamentation in air followed by dispersion compensation. Pulses at a center wavelength of 1040 nm with millijoule pulse energy and 160 fs pulse width from a high-power Yb:CaAlGdO<sub>4</sub> regenerative amplifier are compressed to 32 fs, with only 2.4% loss from the filamentation process. The compressed pulse has a stable output power with a root-mean-square variation of 0.2% over 1 hour.

**Keywords:** femtosecond pulse; filamentation; nonlinear compression

## 1. Introduction

Ultrafast lasers with millijoule pulse energy, tens of watts of average power and a pulse width from a few to a few tens femtoseconds (fs) have found diversified applications, such as the generation of high-order harmonics<sup>[1]</sup>, intrapulse difference-frequency waves<sup>[2]</sup>, terahertz pulses<sup>[3]</sup> and isolated attosecond pulses<sup>[4]</sup>. In the last decade, ytterbium (Yb)-doped lasers have developed rapidly with their superior power scaling capability thanks to the small quantum defects and the availability of high-power laser diodes as the pump source<sup>[5]</sup>, gradually replacing titanium-doped sapphire (Ti:sapphire) lasers, which have long been serving as workhorses of scientific ultrafast lasers. Despite many superior characters, the pulse width of Yb-doped lasers is usually greater than 100 fs<sup>[6]</sup>, limited by the emission bandwidth, which severely hinders the popularization of Yb-doped lasers for the above-mentioned applications.

To further compress the pulse width of Yb-doped lasers, a relatively straightforward strategy is nonlinear pulse

compression, with the principle based on nonlinear spectral broadening and dispersion compensation<sup>[7]</sup>. A number of techniques have been used for nonlinear spectral broadening of millijoule-level Yb-doped lasers<sup>[8–10]</sup>. The hollow core fiber (HCF) technique uses hollow waveguides filled with noble gases to extend the nonlinear interaction length between pulses and a nonlinear medium, which supports the generation of few-cycle pulses with good beam quality<sup>[11]</sup>. However, it is difficult for the transmission efficiency of HCF to exceed 70%<sup>[12–14]</sup>. Careful alignment and good beam pointing of the laser system are also required in HCF compressors. Multiple thin plates using sequences of thin dielectric plates as nonlinear media serve as an effective method for pulse compression with high efficiency<sup>[15–17]</sup>. However, damages to thin plates and beam quality degradation could be an issue for laser system stability and long-term operation. Multi-pass cell (MPC) compressors have proven to be able to achieve extreme compression factors with minimum losses, excellent pointing sensitivity and good beam quality<sup>[18,19]</sup>. However, traditional MPC modules are based on Herriot cavities, which impose relatively complicate beam routings and require delicate dielectric coatings and gas chambers. Filamentation in gases has been adapted over the past decade to achieve ultrashort pulses. Laser filamentation is

Correspondence to: Houkun Liang and Weizhe Wang, College of Electronics and Information Engineering, Sichuan University, Chengdu 610064, China. Emails: [hkliang@scu.edu.cn](mailto:hkliang@scu.edu.cn) (H. Liang); [wangweizhe\\_1997@163.com](mailto:wangweizhe_1997@163.com) (W. Wang)

sustained when the Kerr effect is balanced by diffraction and plasma defocusing<sup>[20]</sup>, which enables much longer non-diffractive propagation compared to the Rayleigh range with a high intensity. As a result, spectral broadening induced by self-phase modulation (SPM) has become more prominent. Equipped with a high-pressure gas cell, 0.68 mJ pulses from a Ti:sapphire laser system with a pulse duration of 33 fs were compressed to 5.1 fs; nevertheless, the optical transmission in two cascaded filaments is only 26% owing to the strong ionization loss<sup>[21]</sup>. In addition, 4 fs pulses were obtained via a single filamentation in a semi-infinite argon gas cell, pumped by 35 fs input pulses with a low compression efficiency<sup>[22]</sup>. Besides the large loss, the strong ionization also induces substantial spatial chirp, and confines the good temporal shape to only the beam center. Without the requirement for vacuum apparatuses nor careful control of the gas pressure, pulse compression through filamentation in air has also been demonstrated, generating 22 fs pulses out of 100 fs input pulses. However, the energy coupled into the inner core of the filament, which generates the spectral broadening, is only 20% of the total input pulse energy, again owing to the strong ionization<sup>[23]</sup>. In addition, the output stability is another important concern in nonlinear pulse compression. Strong ionization and spectral modulation could induce plasma instability<sup>[24,25]</sup>, which should be avoided in the design of Yb-laser compressors.

In this work, a simple, stable and efficient nonlinear pulse compression technique based on cascaded laser

filamentation in air is demonstrated. Pulses with energy of 1 mJ from a Yb-doped laser are compressed from 160 to 32 fs with only 2.4% loss from the filamentation process. The peak power of the Yb-doped laser system is enhanced by approximately four times from 6.25 to 24.7 GW, with good beam quality and spectral homogeneity across the beam profile. The cascaded air filamentation compressor has superior long-term stability, with the measured power variation of less than 0.2% over 1 hour. The demonstrated technique is simple, robust and economical for the efficient pulse compression of Yb-doped lasers with moderate compression factors (five times for two cascaded compression stages), paving the way towards the acquisition of high peak and average power output.

## 2. Results

The configuration of the experimental setup is shown in Figure 1(a). A homemade Yb:CaAlGdO<sub>4</sub> (Yb:CALGO) chirped-pulse regenerative amplifier, generating 160 fs pulses at a central wavelength of 1040 nm and a repetition rate of 20 kHz, is used as the experimental platform. In the experiment, 1 mJ pulses with peak power of 6.25 GW are delivered. The cascaded filamentation compressor consists of two identical modules. Nonlinear spectral broadening is achieved mainly through SPM during the process of laser filamentation in air. Chirped mirrors are placed behind each nonlinear spectral broadening stage to compensate

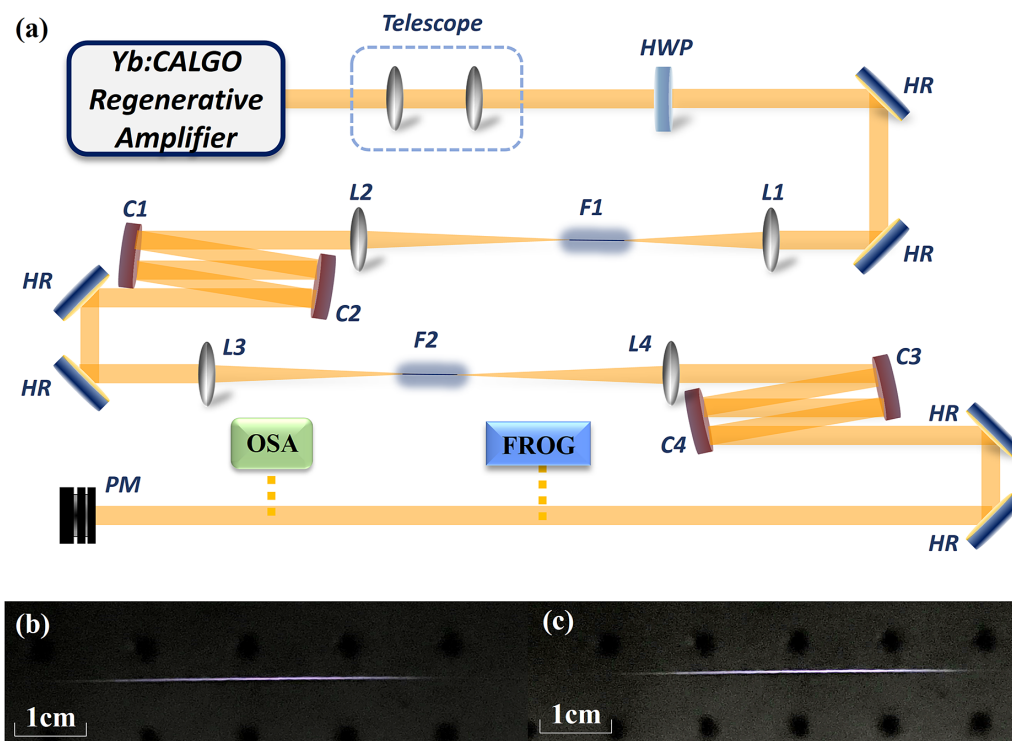


**Figure 1.** (a) Schematic diagram of the cascaded nonlinear compressor through filamentation in air. HWP, half-wave plate; L, lens; C, chirped mirror; F, filamentation; HR, high reflection mirror; PM, power meter. Photos of the generated filamentation in air in the first (b) and second (c) stages.

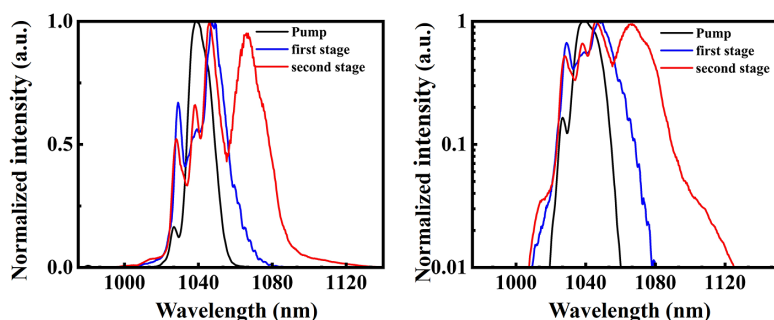


**Figure 2.** Spectra of the input and the output pulses of each nonlinear compression stage in the linear (a) and logarithm (b) scales, respectively. The black, blue and red curves are the pump spectra, the spectra after the first and the second nonlinear compression stages, respectively.

the dispersion. Photos of the laser filamentations from the cascaded modules are shown in Figures 1(b) and 1(c). The laser before and after nonlinear compression is characterized by an optical spectral analyzer (Yokogawa AQ6370D), a power meter (Ophir FL250A-BB-50) and a beam profiler (Dataray WinCamD). The temporal profiles of the compressed pulses are measured by a commercial second-harmonic generation frequency-resolved optical gating (SHG-FROG) setup (Mesa Photonics).

Prior to the nonlinear compressor a telescope system is used to adjust the beam size, which is crucial for maximizing the spectral broadening and at the same time minimizing the ionization loss through the process of laser filamentation. After the telescope, p-polarization is adjusted with a half-wave plate to reduce the polarization loss of the chirped mirrors. In the first compression stage, pulses with an energy of 1 mJ and a peak power of 6.25 GW, which is slightly greater than the critical power of self-focusing in air at a wavelength of 1040 nm, are focused in air by using a lens with 500 mm focal length. Loose focusing is desired for weak ionization and a long interaction length. The beam diameter on the lens is approximately 3.5 mm, generating a linear peak power density of 18.8 TW/cm<sup>2</sup> at the focal spot. As shown in Figure 1(b), a laser filament with a length of approximately 50 mm is formed, through which SPM occurs. The divergent beam is collimated by a lens with a focal length of 750 mm, and the diameter of the collimated beam is approximately 5 mm.

The reason for enlarging the beam size is to avoid damages on the subsequent chirped mirrors. After the collimating lens, the beam is reflected 18 times on the chirped mirror pairs, which provides a total negative dispersion of  $-2700 \text{ fs}^2$  over the spectral range of 850–1200 nm. In the second stage, a lens with a focal length of 750 mm is used to focus the beam, and a filament in air with a length of 55 mm is generated, as shown in Figure 1(c). The peak power density is 36.2 TW/cm<sup>2</sup>. The diverged beam is then collimated by a 750 mm lens and reflected on the chirped mirror pairs for six bounces, which supplies a total negative dispersion of  $-900 \text{ fs}^2$ .

In Figure 2, the spectra of the input and the output pulses of the two nonlinear compression stages are compared in both the linear and logarithm scales. The black and blue curves represent the spectra before and after the first filamentation stage. Spectral broadening spanning from 1010 to 1080 nm at  $-20 \text{ dB}$  is manifested through the first-stage filamentation. The spectrum measured after the second-stage filamentation is shown as red curves in Figure 2, which is significantly broadened compared to the blue ones in both the linear and logarithm scales, covering a spectral range from 1010 to 1130 nm at  $-20 \text{ dB}$ , which supports a transform-limited (TL) pulse width of 30 fs. Notably, in both filamentation stages, the red shift is the main force of spectral broadening, which indicates that in our experiment the spectral broadening is mainly aroused by the Kerr and Raman effects<sup>[26,27]</sup> in air, while the plasma generation associated with ionization loss is weak. It is worth mentioning that when the pulse energy varies in the range of 0.8–1.5 mJ, similar spectral broadening could be achieved by adjusting the beam size on the focusing lens via the telescope.

The temporal profiles of the pump pulse and the pulse after the first and second nonlinear compression stages are characterized by SHG-FROG, as shown in Figure 3. The measured and retrieved FROG traces of the pump pulse are shown in Figures 3(a) and 3(b), respectively. The pump pulse has a bandwidth of 13 nm, as presented in Figure 3(c), which supports a TL pulse of 138 fs. The retrieved temporal profile of the pump pulse indicates a pulse width of 160 fs, as shown in Figure 3(d). The spectral-temporal characteristics of the compressed pulses after the first stage are shown in Figures 3(e)–3(h). The pulse width is compressed from 160 to 65 fs, with a TL pulse width of 58 fs, as manifested in Figure 3(h). The pulse energy after the first nonlinear compression stage is 0.87 mJ, with 85.5% energy contained in the main pulse, generating a peak power of 11.5 GW. In this stage, the losses caused by the filamentation and reflections on the chirped mirrors are 0.8% and 11.6%, respectively. Figures 3(i)–3(l) characterize the second-stage nonlinear compression. The measured and retrieved spectra have a relatively good agreement, as presented

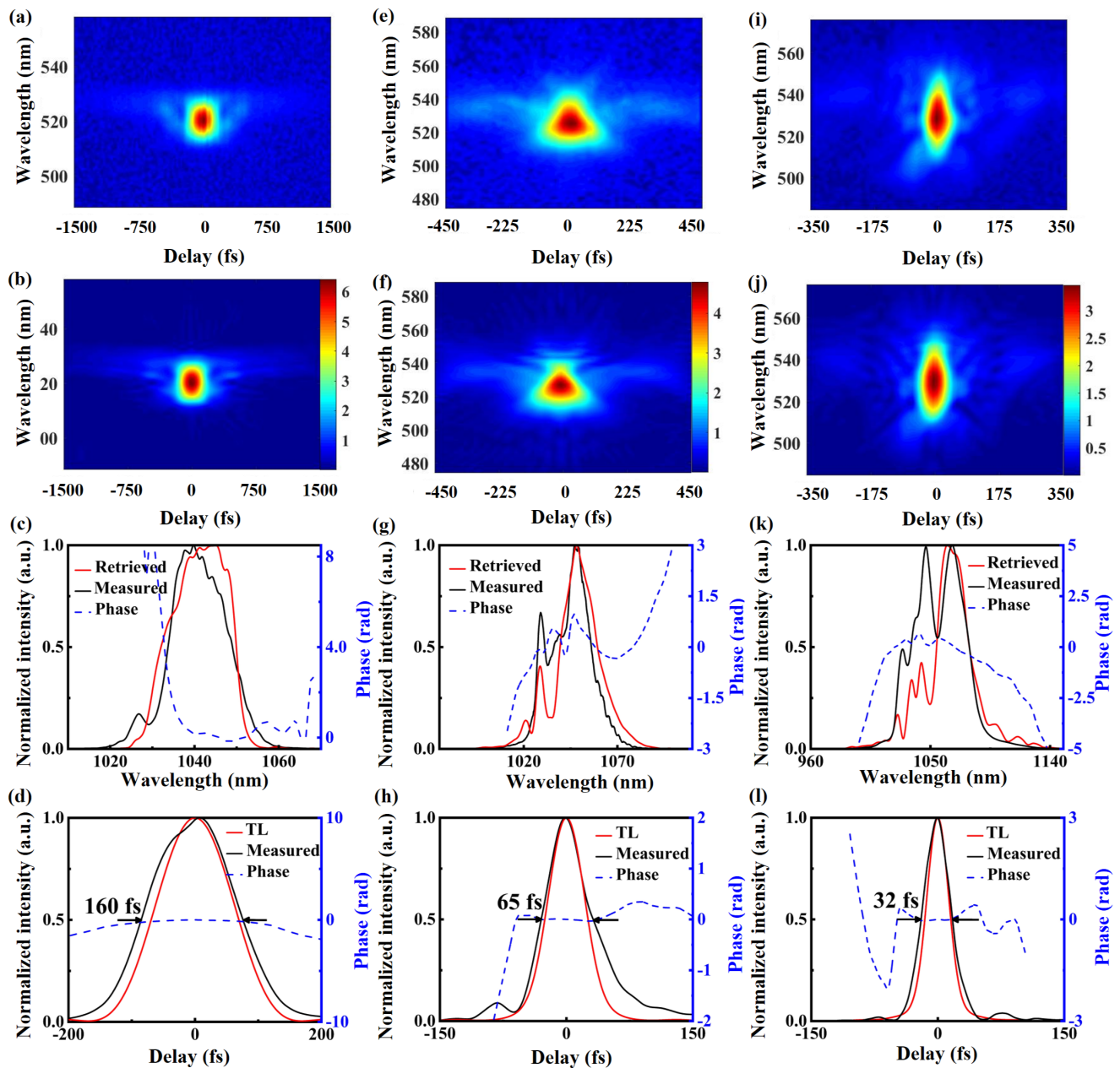


**Figure 3.** SHG-FROG measurements of the 160, 65 and 32 fs pulses from the Yb:CALGO regenerative amplifier, after the first and second compression stages, respectively. Input pulse: the measured (a) and retrieved (b) FROG traces. The FROG error is measured as 0.93%. (c) The retrieved spectral intensity and phase, compared to the spectrum, independently measured using a spectral analyzer. (d) The retrieved and TL temporal profiles indicating a measured pulse width of 160 fs. The pulse from the first compression stage: (e) and (f) are the measured and retrieved FROG traces, respectively. The FROG error is measured as 0.94%. (g) The retrieved spectral intensity and phase, compared to the spectrum independently measured using a spectral analyzer. (h) The retrieved and TL temporal profiles indicating a measured pulse width of 65 fs. The pulse from the second compression stage: (i) and (j) are the measured and retrieved FROG traces, respectively. The FROG error is measured as 1.09%. (k) The retrieved FROG spectral intensity and phase, compared to the spectrum, independently measured using a spectral analyzer. (l) The retrieved and TL temporal profiles indicating a measured pulse width of 32 fs.

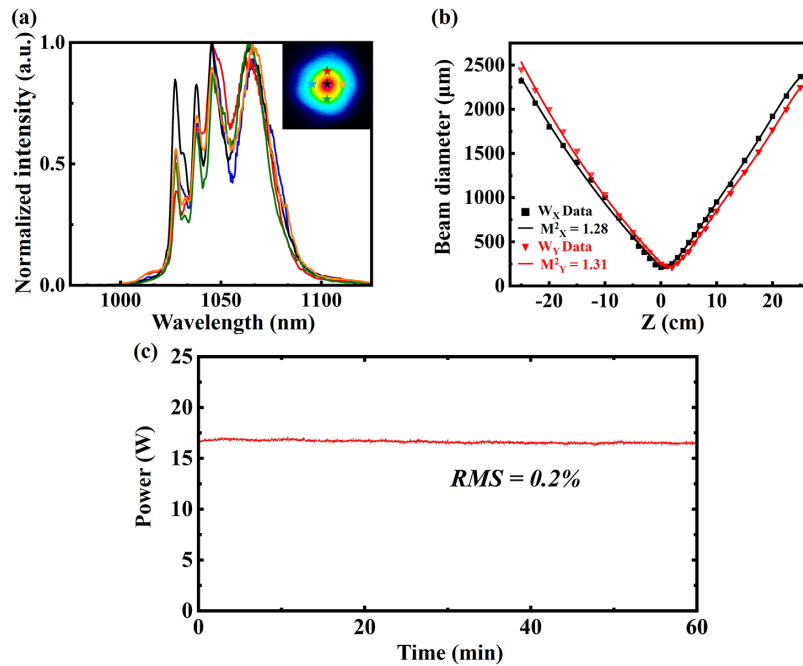
in Figure 3(k). In the second stage, the pulse width is compressed from 65 to 32 fs with a pulse energy of 0.83 mJ. 95% of the total energy is contained in the main pulse, as presented in Figure 3(l), which produces a peak power of 24.7 GW. In the second compression stage, losses from laser filamentation and reflections on the chirped mirrors are measured as 1.6% and 3%, respectively. After both

compression stages the measured and retrieved spectra cannot reproduce the short wavelength sides very well, which is mainly due to the slight misalignment during the FROG trace measurement.

The parameters of the cascaded air filamentation compressor, such as the pulse energy, peak power and efficiency, are summarized in Table 1. After the cascaded air filamentation

**Table 1.** Experimental parameters in the two-stage cascaded air filamentation pulse compressor.

	Input energy	Output energy	Peak power	Loss by filamentation	Total efficiency
First stage	1 mJ	0.87 mJ	11.5 GW	0.8%	87.4%
Second stage	0.87 mJ	0.83 mJ	24.7 GW	1.6%	95.4%

**Figure 4.** (a) The measured spectra at different spatial positions, which are indicated by the five stars across the beam as shown in the inset. (b) Beam quality measurement after nonlinear compression. (c) The measured output power over 1 hour of continuous operation.

compressor, 32 fs pulses with an average power of 16.7 W are obtained and the peak power is increased from 6.25 to 24.7 GW. The compression factors of the first and second stage are 2.45 and 2, respectively. The small nonlinear accumulation and weak ionization process in each compression stage avoid the spatio-temporal inhomogeneity of the laser beam. The total efficiency of the nonlinear compressor is 83% while the loss aroused by laser filamentation is only 2.4%, which indicates that the loss is mainly due to the reflection of the chirped mirrors. It is worth mentioning that limited by the laboratory space and the availability of chirped mirrors, only two stages of the filamentation air compressor are performed in this experiment, but it is foreseeable that by using more stages of air filamentation compressors it is possible to generate sub-10 fs pulses.

The spatial chirp of the output beam after the cascaded air filamentation nonlinear compressor is also characterized, as shown in Figure 4(a). The spectral shapes remain nearly identical when scanning the beam across both axes, which indicates there is almost no spatial chirp resulting from the cascaded filamentation compressor. The  $M^2$ -square ( $M^2$ ) factor of the output beam after two stages of nonlinear compression is characterized in Figure 4(b), revealing values of  $M^2$  of 1.28 and 1.31 along the  $x$ - and  $y$ -axes, respectively. Notably,

the  $M^2$  factors of the pump beam are 1.09 and 1.14 along the  $x$ - and  $y$ -axes, respectively, which indicates that after nonlinear pulse compression the beam quality is only slightly deteriorated. It is therefore evident that the laser output after the cascaded filamentation in air with weak ionization has a good Gaussian beam profile, negligible spatial chirp and small temporal pedestals, which indicates a uniform spatial phase resulting from the nonlinear compression process.

To test the stability of the nonlinear compressor, the laser system is operated for 1 hour with an average power of 16.7 W and a pulse energy of 0.83 mJ after nonlinear compression. Figure 4(c) shows the power stability of the laser output after the cascaded air filamentation compressor. For the measurement time of 1 hour, the root-mean-square (RMS) power variation of approximately 36,000 consecutive points is approximately 0.2%. The slight decreasing trend in average power is caused by the thermal drift of the Yb:CALGO regenerative amplifier. It is worth noting that the nonlinear compression method proposed here, which relies on the cascaded weak ionization, could minimize the plasma instabilities in conventional nonlinear compression techniques and provide a route towards a super-stable and super-efficient nonlinear compression process, especially at high repetition rates.

### 3. Conclusion

In conclusion, we demonstrate a simple, stable and efficient nonlinear pulse compression technique by using cascaded laser filamentation in air. The pulse width from a millijoule Yb:CALGO regenerative amplifier is compressed from 160 to 32 fs, with a total transmission efficiency of 83%, in which the loss arising from filamentation is only 2.4%, and the major loss is from the reflection of the chirped mirrors. Thus, a peak power of 24.7 GW is achieved. Moreover, the demonstrated technique has a superior stability with a measured output power variation of 0.2% over 1 hour. It is worth noting that with more stages of the air filamentation compressor, it is possible to obtain sub-10 fs pulses with high efficiency by using customized chirped mirrors. Compared to MPC, HCF and multi-plate compressors, fine alignment of the pump beam and precise pressure control of the gas chambers are not required. In addition, there is no risk of damaging the optical components such as the HCF and thin plates in the nonlinear compressor. Therefore, we believe the developed cascaded air filamentation compressor can provide a new route for generating high-energy pulses with a pulse width of 10–30 fs, which can extend the applications of Yb-doped lasers, such as high harmonic generation and terahertz rectification.

### References

1. T. Popmintchev, M. C. Chen, D. Popmintchev, P. Arpin, S. Brown, S. Ališauskas, G. Andriukaitis, T. Balčiūnas, O. D. Mücke, A. Pugzlys, A. Baltuška, B. Shim, S. E. Schrauth, A. Gaeta, C. H. García, L. Plaja, A. Becker, A. J. Becker, M. M. Murnane, and H. C. Kapteyn, *Science* **336**, 1287 (2012).
2. I. Pupeza, D. Sánchez, J. Zhang, N. Lilienfein, M. Seidel, N. Karpowicz, T. Paasch-Colberg, I. Znakovskaya, M. Pescher, W. Schweinberger, V. Pervak, E. Fill, O. Pronin, Z. Wei, F. Krausz, A. Apolonski, and J. Biegert, *Nat. Photonics* **9**, 721 (2015).
3. B. Zhang, Z. Ma, J. Ma, X. Wu, C. Ouyang, D. Kong, T. Hong, X. Wang, P. Yang, L. Chen, Y. Li, and J. Zhang, *Laser Photon. Rev.* **15**, 2000295 (2021).
4. T. Gaumnitz, A. Jain, Y. Pertot, M. Huppert, I. Jordan, F. A. Lamas, and H. J. Wörner, *Opt. Express* **25**, 27506 (2017).
5. Y. Wang, H. Chi, C. Baumgarten, K. Dehne, A. R. Meadows, A. Davenport, G. Murray, B. A. Reagan, C. S. Menoni, and J. J. Rocca, *Opt. Lett.* **45**, 6615 (2020).
6. R. Caracciolo, M. Kemnitzer, A. Guandalini, F. Pirzio, A. Agnesi, and J. Aus der Au, *Opt. Express* **22**, 19912 (2014).
7. T. Nagy, P. Simon, and L. Veisz, *Adv. Phys. X* **6**, 1845795 (2021).
8. R. Piccoli, A. Rovere, Y. G. Jeong, Y. Jia, L. Zanutto, F. Légaré, B. E. Schmidt, R. Morandotti, and L. Razzari, *Opt. Express* **27**, 32659 (2019).
9. C. H. Lu, W. H. Wu, S. H. Kuo, J. Y. Guo, M. C. Chen, S. D. Yang, and A. H. Kung, *Opt. Express* **27**, 15638 (2019).
10. M. Kaumanns, V. Pervak, D. Korman, V. Leshchenko, A. Kessel, M. Ueffing, M. Chen, and T. Nubbemeyer, *Opt. Lett.* **43**, 5877 (2018).
11. M. Ouillé, A. Vernier, F. Böhle, F. M. Bocoum, A. Jullien, M. Lozano, J. P. Rousseau, Z. Cheng, D. Gustas, A. Blumenstein, P. Simon, S. Haessler, J. Faure, T. Nagy, and R. Lopez-Martens, *Light Sci. Appl.* **9**, 47 (2020).
12. E. Haddad, R. Safaei, A. Leblanc, R. Piccoli, Y. G. Jeong, H. Ibrahim, B. E. Schmidt, R. Morandotti, L. Razzari, F. Légaré, and P. Lassonde, *Opt. Express* **26**, 25426 (2018).
13. T. Nagy, S. Hädrich, P. Simon, A. Blumenstein, N. Walther, R. Klas, J. Buldt, H. Stark, S. Breitkopf, P. Jójárt, I. Seres, Z. Várallyay, T. Eidam, and J. Limpert, *Optica* **6**, 1423 (2019).
14. R. Klas, W. Eschen, A. Kirsche, J. Rothhardt, and J. Limpert, *Opt. Express* **28**, 6188 (2020).
15. J. Guo, Z. Gao, D. Sun, X. Du, Y. Gao, and X. Liang, *High Power Laser Sci. Eng.* **10**, E10 (2021).
16. W. Z. Wang, T. Pu, H. Wu, Y. Li, R. Wang, B. Sun, and H. K. Liang, *Opt. Express* **30**, 22153 (2022).
17. S. Zhang, Z. Fu, B. Zhu, G. Fan, Y. Chen, S. Wang, Y. Liu, A. Baltuska, C. Jin, C. Tian, and Z. Tao, *Light Sci. Appl.* **10**, 53 (2021).
18. P. Balla, A. B. Wahid, I. Sytceвич, G. Chen, A. L. Viotti, L. Silletti, A. Cartella, S. Alisauskas, H. Tavakol, G. W. Uwe, A. Schönberg, M. Seidel, A. Trabattoni, B. Manschwetus, L. Tino, F. Calegari, A. Couairon, A. L'Huillier, C. L. Arnold, I. Hartl, and C. M. Heyl, *Opt. Lett.* **45**, 2572 (2020).
19. M. Hanna, F. Guichard, N. Daher, Q. Bournet, X. Délen, and P. Georges, *Laser Photon. Rev.* **15**, 2100220 (2021).
20. A. Couairon and A. Mysyrowicz, *Phys. Rep.* **441**, 47 (2007).
21. C. P. Hauri, A. Guandalini, P. Eckle, W. Kornelis, J. Biegert, and U. Keller, *Opt. Express* **13**, 7541 (2005).
22. D. S. Steingrube, M. Kretschmar, D. Hoff, E. Schulz, T. Binhammer, P. Hansinger, G. G. Paulus, U. Morgner, and M. Kovacev, *Opt. Express* **20**, 24049 (2012).
23. O. Varela, B. Alonso, I. J. Sola, J. S. Román, A. Zaïr, C. Méndez, and L. Roso, *Opt. Lett.* **35**, 3649 (2010).
24. Y. Kato, K. Mima, N. Miyanaga, S. Arinaga, Y. Kitagawa, M. Nakatsuka, and C. Yamanaka, *Phys. Rev. Lett.* **53**, 1057 (1984).
25. E. M. Epperlein, *Phys. Rev. Lett.* **65**, 2145 (1990).
26. V. Carlo, S. Mostafa, K. Aleksandr, L. Leonid, and P. H. Christoph, *Opt. Lett.* **41**, 4719 (2016).
27. P. A. Carpeggiani, G. Coccia, G. Fan, E. Kaksis, A. Pugžlys, A. Baltuška, R. Piccoli, Y.-G. Jeong, A. Rovere, R. Morandotti, L. Razzari, B. E. Schmidt, A. A. Voronin, and A. M. Zheltikov, *Optica* **7**, 1349 (2020).